University of Glasgow

Budday, S. and Steinmann, P. (2018) On the influence of inhomogeneous stiffness and growth on mechanical instabilities in the developing brain.*International Journal of Solids and Structures*, 132-33, pp. 31-41. (doi:10.1016/j.ijsolstr.2017.08.010)

There may be differences between this version and the published version. You are advised to consult the publisher's version if you wish to cite from it.

http://eprints.gla.ac.uk/185713/

Deposited on: 13 June 2019

Enlighten – Research publications by members of the University of Glasgow
http://eprints.gla.ac.uk

On the influence of inhomogeneous stiffness and growth on mechanical instabilities in the developing brain

Silvia Budday[a,*], Paul Steinmann[a]

[a] *Chair of Applied Mechanics, Department of Mechanical Engineering, University of Erlangen-Nrnberg, Egerlandstr. 5, 91058 Erlangen, Germany, email: silvia.budday / paul.steinmann@fau.de*

Abstract

The characteristic surface morphology of the mammalian brain is closely correlated with brain function and dysfunction. During development, the initially smooth surface evolves into an elaborately convoluted pattern. Growing evidence suggests that mechanical instabilities emerging from differential growth between a faster growing outer gray matter and a slower growing inner white matter play a major role in brain morphogenesis. Previous studies assume uniform growth and stiffness; yet, recent experiments indicate that the properties of brain tissue are highly inhomogeneous. Here, we hypothesize that regionally varying developmental pathways across the brain result in nonuniform material properties at the onset of cortical folding. We establish a computational model of brain growth to explore the effects of stiffness and growth variations in gray and white matter tissue to mimic cellular processes and evolving tissue microstructure. We present an effective approach to determine critical growth values from geometrical data and systematically study the effect of inhomogeneous material properties on growth-induced primary and secondary instabilities. Our results reveal that critical growth and wavelength strongly depend on the stiffness distribution in the developing brain. Regional variations in cortical growth affect secondary instabilities and evoke highly irregular folding patterns, but characteristic wavelength and critical growth remain relatively stable. The interplay of different influential factors including cortical thickness, brain geometry, stiffness, and growth explains how primary folds are highly preserved across individuals, whereas secondary and tertiary folds vary significantly. Our findings are directly applicable to imaging data of fetal brains and ultimately enable early diagnostics of cortical malformations to improve treatment of neurodevelopmental disorders including epilepsy, autism, spectrum disorders, and schizophrenia.

Keywords: cortical folding; growth; instabilities; period-doubling; inhomogeneous properties

1. Introduction

The mechanisms that drive the formation of cortical convolutions during brain development have recently caught the attention of researchers in various fields. First studies suggesting that mechanics play an important role during brain development [20, 40] had long fallen into oblivion. Recent evidence, however, has strikingly strengthened the mechanically motivated hypothesis that growth-induced mechanical instabilities drive cortical folding as the outer gray matter, the cortex, grows much faster than the inner white matter. Constraint cortical growth leads to compressive stresses high enough to induce surface buckling. Analytical [40], numerical [3, 39], and experimental [47] predictions agree well with anatomical observations [20] including classical malformations associated with neurological disorders such as schizophrenia and autism [8]. The mechanical model further explains the occurrence of period-doubling patterns as shown in Figure 1. Previous studies have mostly assumed homogeneous properties within the different layers although it is well known that the microstructure of brain tissue is highly inhomogeneous [9]. While we can macroscopically distinguish between two main tissue types, gray matter and white matter, recent experimental evidence indicates that the microscopic structure and material properties can vary significantly even within those regions [17, 52]. This most likely applies to the highly dynamic developmental stage in particular. Furthermore, homogeneous stiffness and growth in the cortex fail to explain why primary folds are highly consistent among individuals [37, 55]. To elucidate the influence of inhomogeneities in material properties on cortical folding, we consider the cellular processes during brain development and systematically study inhomogeneous stiffness and growth distributions. We present an effective geometrical approach to assess growth-induced instabilities in highly irregular systems and indicate how inhomogeneous growth could explain highly preserved primary folds and more variable secondary and tertiary folds.

Although great efforts have been made to characterize the mechanical behavior of mature brain tissue [24, 43, 25, 9], the stiffness of the fetal brain remains unknown [16]. Regarding its microstructure, during the early stages of development progenitor cells in the

*corresponding author.

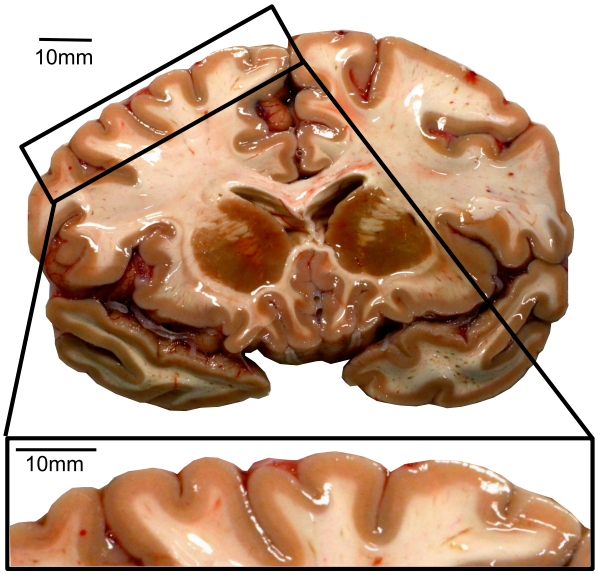

Figure 1: Folding pattern on a coronal slice of a human brain, constructed from the same raw image as in [9]. Secondary period-doubling patterns are clearly visible.

deep ventricular and subventricular zones divide to generate neurons which migrate outwards through the cell-sparse intermediate zone to form the cortex from inside out [14, 44]. When cortical cells mature and form inter- and intracortical connections [38], the brain surface expands and begins to fold [41, 12]. Simultaneously, the vascular system develops, which closely correlates with cell proliferation and connectivity. The vasculature follows the radial gradient from the inside to the outside and is first limited to the deep proliferating ventricular and subventricular zones before it progresses through the intermediate zone, the subplate, and toward the surface. As recent experiments on mature human brains suggest that factors such as capillary density and brain activity correlate with the elastic properties of the tissue [9], we hypothesize that the stiffness at the onset of cortical folding is not uniform. Rather, it likely correlates with the developmental gradient in radial direction: deep proliferating layers and the cortex with high density of cell nuclei and capillaries might be stiffer than the cell-sparse intermediate layers as illustrated in Figure 2.

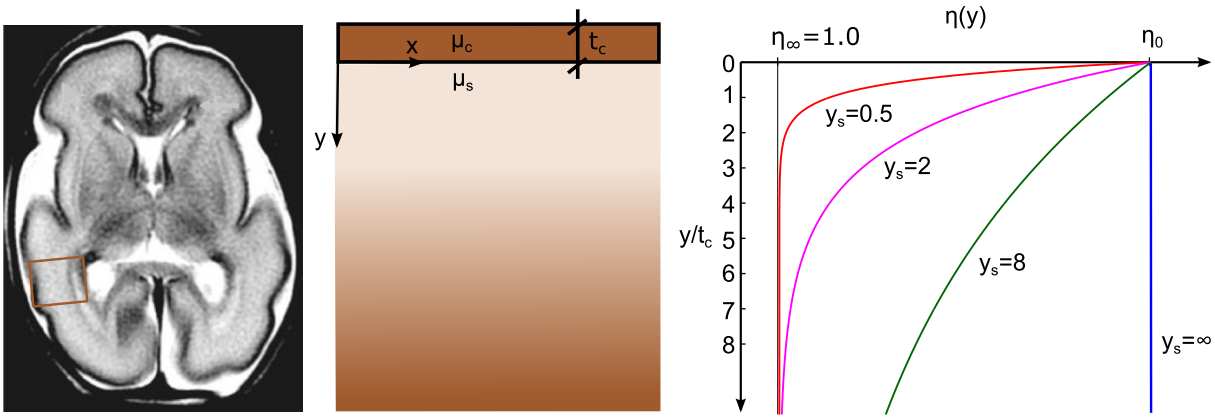

Figure 2: Brain development follows a radial gradient from inside out. As elastic properties of brain tissue correlate with brain activity, neuronal connectivity, and capillary density, we approximate the stiffness distribution in the developing subcortex by an exponential function, where the deep proliferating zones are stiffer than the cell-sparse intermediate layers. We assume that the stiffness contrast between cortex and subcortex, $\eta(y) = \mu_c/\mu_s(y)$, increases exponentially with depth y as $\eta(y) = \eta_\infty + [\eta_0 - \eta_\infty] \exp(-y/y_s)$ in terms of the stiffness contrasts at the boundary η_0 and at infinity $\eta_\infty = 1$, scaled by the parameter y_s. The structural gradient in the developing subcortex can also be deduced from the magnetic resonance image of a very preterm neonate at 27 weeks of gestation (left), adapted from [8].

Not only the stiffness might vary across the developing fetal brain but also cortical growth rates. It has been observed that the subventricular and ventricular zones are thicker at sites of evolving gyri and thinner beneath sulci. Similarly, the cortex is thicker in the crowns of gyri than in sulci [33]. Thicker proliferating zones could lead to increased cell migration and higher growth rates. Therefore, we pose the question whether cortical folding patterns are partially driven by local variations in both cortical stiffness

and growth rates [12] and systematically study the effect of inhomogeneous properties on the evolving folding pattern.

In a first approximation, cortical folding can be considered as the instability problem of a thin, uniaxially growing stiff film resting on a homogeneous soft, infinitely deep substrate. Then, a linear perturbation analysis provides closed-form estimates for the critical growth and critical wavelength for periodic wrinkling [5, 3, 11]. Independent of cortical folding, the influence of inhomogeneous substrate stiffness on buckling phenomena has previously been investigated analytically and numerically assuming simplified geometries and exponential or power-law gradients in the radial direction [36, 15] or step-like functions in the circumferential direction [1]. Irregular geometries as well as more complex stiffness and growth distributions as those we expect in the developing brain, to the authors awareness, require numerical treatment. Furthermore, analytical considerations fail to provide information about the evolution of the surface morphology in the highly nonlinear post-buckling regime. Thus, in the current study we perform finite element simulations to investigate the influence of spatially varying stiffness and growth on the onset of primary wrinkling and the evolution of secondary wrinkling phenomena. However, the identification of critical conditions for buckling instabilities within a finite element setup is not trivial [32]. Possible approaches include an accompanying eigenvalue analysis [31] or tracing the evolution of neighboring amplitudes with growth [7]. The former is a rather theoretical approach and not readily comparable to experimental data such as Magnetic Resonance Images, while the latter requires well defined gyri and sulci which are stable in time. Here, we evaluate geometrical data, the evolution of amplitudes and mean cortical thicknesses, to characterize growth-induced primary and secondary instabilities in the inhomogeneous developing brain. With the rapid enhancement of in utero imaging techniques, the presented approach could ultimately enable the analysis of growth-induced instabilities in the fetal brain from imaging data.

Previous studies on cortical folding have indicated possible effects of non-uniform cortical growth on pattern selection [3, 39, 55], but only considered imposed patterns close to the characteristic pattern. They compared final folding patterns without considering the effects on critical conditions for primary and secondary instabilities referring to the possible underlying mechanisms on the cellular level. In this study, we assess the influence of inhomogeneous material properties based on the cellular processes during brain development. We discuss critical conditions for primary and secondary instabilities as well as the evolution of the surface morphology to provide a systematic understanding of the underlying instability. We evaluate to which extent local variations in stiffness, cortical growth, and cortical thickness affect pattern selection in the developing brain. We show how those effects may correlate with the highly consistent primary folds and much more variable secondary and tertiary folds in the human brain. The current study is not only relevant for brain folding, but it applies to any biological system where local variations in properties control growth-induced instabilities and affect pattern selection.

2. Growth model

To explore the effect of inhomogeneous stiffness and growth distributions on the folding evolution in the developing brain, we perform finite element simulations using the non-linear field theories of mechanics supplemented by the theory of finite growth [11]. A set of only five equations defines the kinematics, the constitutive behavior, the mechanical equilibrium, the growth kinematics, and the growth kinetics. We introduce the deformation map $\boldsymbol{\varphi}$, which maps points $\boldsymbol{X}$ from the undeformed configuration to their new positions $\boldsymbol{x} = \boldsymbol{\varphi}(\boldsymbol{X}, t)$ in the deformed configuration. We further multiplicatively decompose the defomation gradtient $\boldsymbol{F}$ and the Jacobian J into an elastic part and a growth part [26],

$$\boldsymbol{F} = \nabla_{\boldsymbol{X}} \boldsymbol{\varphi} = \boldsymbol{F}^{\mathrm{e}} \cdot \boldsymbol{F}^{\mathrm{g}} \qquad \text{and} \qquad J = \det(\boldsymbol{F}) = J^{\mathrm{e}}\, J^{\mathrm{g}}\,. \tag{1}$$

To define the kinematics of growth, the growth tensor $\boldsymbol{F}^{\mathrm{g}}$, we consider cellular mechanisms during brain development [12]. Cortical folding occurs after neuronal migration has ceased and the vast majority of neurons has already reached its final destination in the cortex, simultaneously with neuronal maturation: neurons form numerous intra- and intercortical connections [38] and establish a dense network incorporating glial cells and capillaries, which leads to a significant volume expansion [12]. Based on these cellular processes, we assume that growth is isotropic, parameterized in terms of a single scalar-valued growth multiplier ϑ,

$$\boldsymbol{F}^{\mathrm{g}} = \vartheta\, \boldsymbol{I} \qquad \text{and} \qquad J^{\mathrm{g}} = \det(\boldsymbol{F}^{\mathrm{g}}) = \vartheta^3\,. \tag{2}$$

This implies that the grown volume J^{g} is identical to the growth multiplier cubed ϑ^3. We characterize the constitutive behavior of the cortex and the subcortex through the following Neo-Hookean free energy parameterized exclusively in terms of the elastic tensor $\boldsymbol{F}^{\mathrm{e}} = \boldsymbol{F} \,/\, \vartheta$ and its Jacobian $J^{\mathrm{e}} = J \,/\, \vartheta^3$, as

$$\psi(\boldsymbol{F}^{\mathrm{e}}) = \frac{1}{2}\,\lambda\, \ln^2(J^{\mathrm{e}}) + \frac{1}{2}\,\mu\,[\,\boldsymbol{F}^{\mathrm{e}} \colon \boldsymbol{F}^{\mathrm{e}} - 3 - 2\,\ln(J^{\mathrm{e}})\,]\,, \tag{3}$$

where λ and μ are the Lamé constants. This implies that only the elastic part of the deformation induces stress. Following standard arguments of thermodynamics, the Piola stress $\boldsymbol{P}$ follows as energetically conjugate to the deformation gradient $\boldsymbol{F}$,

$$\boldsymbol{P} = \frac{\partial \psi(\boldsymbol{F}^{\mathrm{e}})}{\partial \boldsymbol{F}} = \frac{\partial \psi(\boldsymbol{F}^{\mathrm{e}})}{\partial \boldsymbol{F}^{\mathrm{e}}} : \frac{\partial \boldsymbol{F}^{\mathrm{e}}}{\partial \boldsymbol{F}} = \boldsymbol{P}^{\mathrm{e}} \cdot \boldsymbol{F}^{\mathrm{g-t}} = \frac{1}{\vartheta}\boldsymbol{P}^{\mathrm{e}} = \frac{1}{\vartheta^2}\,\mu\,\boldsymbol{F} + \left[\,\lambda\,\ln\!\left(\frac{J}{\vartheta^3}\right) - \mu\,\right]\boldsymbol{F}^{-\mathrm{t}}\,. \tag{4}$$

The Piola stress enters the standard balance of linear momentum, the equation of mechanical equilibrium. In the absence of volume forces, the balance of linear momentum reduces to the vanishing divergence of the Piola stress,

$$\text{Div}\, \boldsymbol{P} \doteq \boldsymbol{0}\,. \tag{5}$$

It remains to define the kinetics of growth, the equations that characterize the evolution of the growth multiplier in time. Since the cortex consists primarily of cell nuclei whereas the subcortex consists primarily of axons, we assume different growth kinetics for the cortex and subcortex. For the cortex, we assume that growth is purely morphogenetic [2], characterized exclusively by the growth rate G_c,

$$\dot{\vartheta} = G_c\,. \tag{6}$$

We let the cortex grow linearly in time, $G_c = \text{const}$. In the case of inhomogeneous cortical growth, G_c varies in space dependent on regional variations in cell proliferation. For the subcortex, we assume that growth is stretch-induced [8]. The buckling instability of the cortex induces extreme deformations to cells in the subcortex, which lengthen gradually when subject to chronic stretch [6]. We make the following ansatz,

$$\dot{\vartheta} = G_s \langle\, J^e - J^0 \,\rangle = G_s \langle\, J \,/\, \vartheta^3 - J^0 \,\rangle\,, \tag{7}$$

where G_s is the subcortical growth rate. The term in the Macaulay brackets $\langle\, J^e - J^0 \,\rangle$ activates growth only if the elastic volume stretch J^e exceeds its baseline value J^0, i.e., when axons are stretched beyond their physiological limit [21].

3. Simulation results

3.1. A geometrical approach to assess critical conditions for primary and secondary instabilities

Figure 3 shows the evolution of a period-doubling pattern that emerges when the cortex grows morphogenetically on a stretch-induced growing substrate for a two-dimensional rectangular simulation domain. We discretize the domain with 2.5 elements per mm in $x-$ and $y-$directions, respectively. This results in a minimum of 24 elements per wavelength, which was found to ensure adequate results (agreeing with analytical predictions for uniform material properties [11]) when using linear finite elements. We choose a domain size that is twice the characteristic wavelength - the critical wavelength for primary wrinkling λ^{crit} - and impose a small kinematic imperfection within a narrow band of two elements in the middle of the domain, small enough not to affect the overall results. With this setting, we have previously shown that we could evoke a variety of secondary folding patterns including period-tripling or period-quadrupling by careful choice of boundary conditions [7]. In this study, however, we only focus on period-doubling as the favorable mode [7] to closely mimic the folding pattern in the human brain shown in Figure 1.

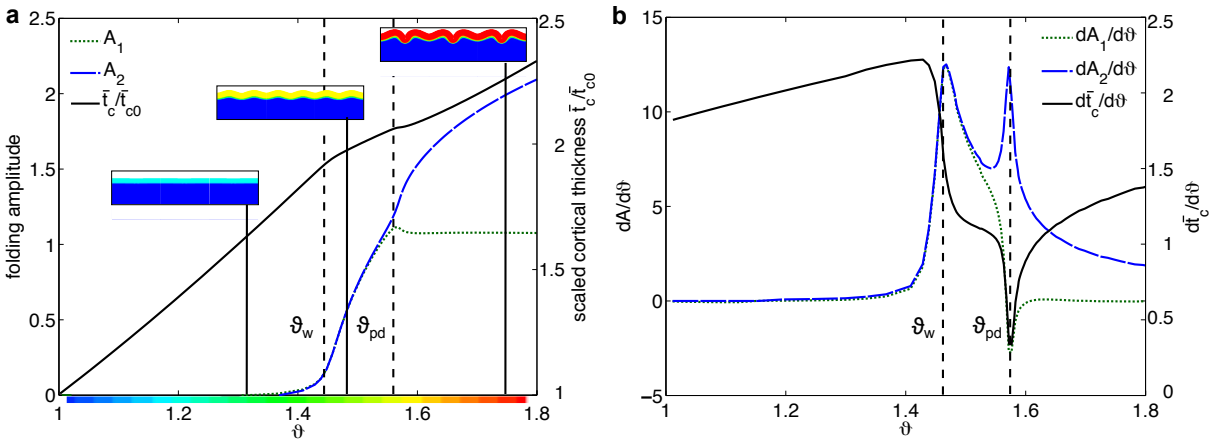

Figure 3: Primary and secondary bifurcations of a morphogenetically growing cortex on a stretch-induced growing subcortex. a) Initially, the cortex is flat, the amplitudes equal zero, and the mean cortical thickness scaled by its initial value increases linearly with growth ϑ. At a first instability point ϑ_w, amplitudes A_1 and A_2 begin to grow simultaneously shown in blue and green and the evolution of the scaled mean cortical thickness $\bar{t}_c/\bar{t}_{c0}$ in black shows a kink - the increase in cortical thickness slows down. At the second instability point ϑ_{pd}, a pitchfork bifurcation occurs regarding the amplitudes, where every second amplitude grows and those in between decay. The cortical thickness briefly remains constant before it increases at its former rate. b) The derivatives of the evolution of amplitudes and mean cortical thickness with respect to growth ϑ allow to distinctly identify the first and second critical growth values: ϑ_w is the first maximum of $dA_{1/2}/d\vartheta$ and the first inflection of $d\bar{t}_c/d\vartheta$, while ϑ_{pd} is the minimum or second maximum of $dA_1/d\vartheta$ and $dA_2/d\vartheta$, respectively, and the minimum of $d\bar{t}_c/d\vartheta$.

Figure 3a shows the evolution of the neighboring amplitudes A_1 and A_2 and the mean cortical thickness scaled by the initial cortical thickness $\bar{t}_c/\bar{t}_{c0}$ with growth ϑ. At a first instability point ϑ_w, the initially flat cortex buckles into a wavy pattern and

amplitudes grow uniformly. The mean cortical thickness shows a kink. At a second instability point ϑ_{pd}, the wrinkled pattern further bifurcates into a period-doubling mode, where only every second amplitude continues to grow, while those in between flatten. During the secondary instability the mean thickness briefly remains constant before it further increases at the same rate as before.

While the evolution of amplitudes immediately allows us to determine the critical growth for periodic wrinkling and period-doubling [7], for the evolution of the mean cortical thickness, the instability points are less obvious. The latter, however, is an easily accessable measure in highly inhomogeneous systems, where the folding pattern is highly irregular or unstable in time. Thus, to identify the critical conditions from the mean cortical thickness, we additionally plot the rate of change of cortical thickness and folding amplitudes with respect to the cortical growth multiplier ϑ, $\mathrm{d}\bar{t}_{\mathrm{c}}/\mathrm{d}\vartheta$ and $\mathrm{d}A_{1/2}/\mathrm{d}\vartheta$, in Figure 3b. This graph reveals several characteristics of primary and secondary bifurcations. The first instability occurs at the first maximum of $\mathrm{d}A_1/\mathrm{d}\vartheta$ and $\mathrm{d}A_2/\mathrm{d}\vartheta$. This point corresponds to the first inflection of $\mathrm{d}\bar{t}_{\mathrm{c}}/\mathrm{d}\vartheta$ at which the curve changes from being convex to concave. We note that we observe a certain rise of amplitudes in Figure 3a even before the instability point ϑ_{w} is reached. This can be attributed to the small kinematic imperfection, which is perceptible slightly before the system becomes unstable. While this perturbation is required to ensure consistent initiation of folding on the otherwise perfectly regular simulation domain, it does not affect the critical conditions for instabilities. At the second instability point, $\mathrm{d}A_2/\mathrm{d}\vartheta$ and $\mathrm{d}\bar{t}_{\mathrm{c}}/\mathrm{d}\vartheta$ reach a minimum, while $\mathrm{d}A_1/\mathrm{d}\vartheta$ reaches a second maximum. Only the first instability, periodic wrinkling, permanently relaxes the compression in the cortex: $\mathrm{d}\bar{t}_{\mathrm{c}}/\mathrm{d}\vartheta$ decreases as the compression in the cortex is partially released. At the second instability point, where the wrinkled surface further bifurcates into a period-doubling mode, $\mathrm{d}\bar{t}_{\mathrm{c}}/\mathrm{d}\vartheta$ reduces to its minimum but immediately comes back to the rate during periodic wrinkling. This suggests that the second instability is not associated with a permanent change in the energy of the layer. While periodic wrinkling releases compression in the cortex, secondary period-doubling minimizes compression in the subcortex.

Geometric quantities as plotted in Figure 3 allow us to identify critical conditions for growth-induced instabilities and also provide indication about their energetic causation. In simple homogeneous systems, the evolution of neighboring amplitudes is a convenient to assess measure to characterize growth-induced primary and secondary instabilities. In highly inhomogeneous systems, the thickness evolution, which we will further analyze in Section 3.4 represents a suitable alternative.

3.2. Inhomogeneous stiffness distribution in the subcortex

Regarding cellular processes during brain development [12] in combination with recent experimental evidence suggesting that elastic properties of brain tissue correlate with capillary density, intercellular connections, and brain activity, we suppose that the stiffness in the developing subcortical white matter is not uniform but increases from the cell-sparse intermediate layers just beneath the developing cortex towards the deep proliferating zones with higher relative cell density [42] as indicated in Figure 2. We approximate the stiffness contrast between cortex and subcortex, $\eta(y) = \mu_{\mathrm{c}}/\mu_{\mathrm{s}}(y)$, by an exponential function,

$$\eta(y) = \frac{\mu_{\mathrm{c}}}{\mu_{\mathrm{s}}(y)} = \eta_\infty + [\,\eta_0 - \eta_\infty\,]\,\exp(-y/y_{\mathrm{s}}), \tag{8}$$

in terms of the stiffness contrast at the cortical-subcortical interface, $\eta_0 = (\mu_{\mathrm{c}}/\mu_{\mathrm{s}})_0$, the stiffness contrast at infinite depth $y \to \infty$, η_∞, and the scaling parameter y_{s} that quantifies the stiffness decay in the substrate. We further assume that the cortical stiffness remains constant $\mu_{\mathrm{c}} = \text{const.}$ and that $\eta_\infty = 1$. In what follows, we analyze two different geometries: the two-dimensional rectangular domain from Section 3.1, which is easily comparable to the analytical solution for uniform material properties, and a three-dimensional hollow ellipsoid, which represents an idealized brain with ventricular cavity.

Figure 4 illustrates the effects of an exponential stiffness distribution in the subcortex on the folding wavelength in Figure 4a and the critical growth for primary and secondary instabilities in Figure 4b. The wavelength of folds increases when the stiffness of the subcortex decreases relative to the stiffness of the cortex corresponding to increasing $(\mu_{\mathrm{c}}/\mu_{\mathrm{s}})_0$ and increasing y_{s}, see Figure 4a and c. The critical growth for primary wrinkling ϑ_{w} denoted by dots in Figure 4b decreases asymptotically with increasing stiffness contrast at the cortical-subcortical interface $(\mu_{\mathrm{c}}/\mu_{\mathrm{s}})_0$ and increases with decreasing y_{s}. The critical growth for period-doubling ϑ_{pd} denoted by diamonds shows a slight increase with $(\mu_{\mathrm{c}}/\mu_{\mathrm{s}})_0$ evoked by stretch-induced growth in the substrate [13] stabilizing the post-wrinkling evolution. Similar to ϑ_{w}, ϑ_{pd} increases with decreasing y_{s}. Stretch-induced growth in the substrate gains influence with increasing folding amplitudes and thus ϑ_{pd} particularly increases for high values of y_{s} and $(\mu_{\mathrm{c}}/\mu_{\mathrm{s}})_0$. This explains why the curves corresponding to $y_{\mathrm{s}} = 0.5$ and $y_{\mathrm{s}} = 2.0$ in red and magenta intersect with $y_{\mathrm{s}} = 8.0$ in green for high stiffness contrasts. Notably, for $y_{\mathrm{s}} = 0.5$, amplitudes remain too small to induce a relevant amount of growth in the subcortex and the second instability point appears independent of $(\mu_{\mathrm{c}}/\mu_{\mathrm{s}})_0$, which coincides with the wrinkling behavior on a non-growing substrate [7].

We suppose that when the stiffness contrasts $(\mu_{\mathrm{c}}/\mu_{\mathrm{s}})_0$ decrease below the value where primary and secondary critical growth in Figure 4b intersect, periodic wrinkling is not necessarily the favorable mode of instability any more. We can still evoke periodic wrinkles within the computational framework presented here and determine the corresponding critical growth. However, cusped sulci form, which transition into folds with self-contact before period-doubling is induced. Thus, analytical solutions based on a sinusoidal wrinkling pattern [11] are no longer valid. The actual surface pattern is not sinusoidal but alternative instability modes become favorable and occur at lower growth values than wrinkling [28]. Highly localized instability modes such as creasing are

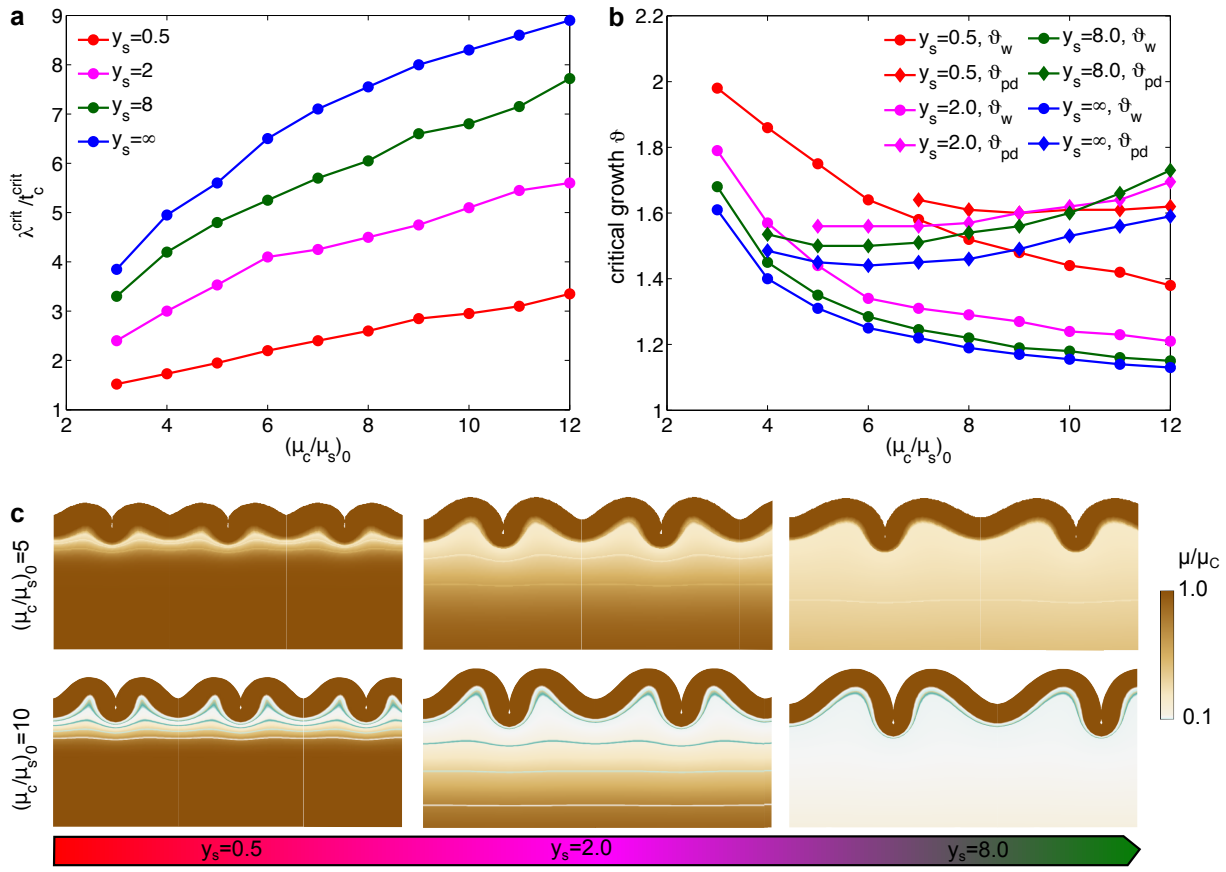

Figure 4: Sensitivity of surface morphology (c), critical wavelength (a) and critical growth (b) with respect to stiffness gradient in the substrate as a function of the stiffness contrast $(\mu_c/\mu_s)_0$ at the cortical-subcortical interface on a rectangular two-dimensional simulation domain. The critical wavelength increases with increasing stiffness contrast and increasing parameter y_s. The primary critical condition for periodic wrinkling illustrated by dots decreases asymptotically with inreasing stiffness contrast; the secondary critical condition for period-doubling illustrated by diamonds marginally increases with increasing stiffness contrast. Both primary and secondary critical conditions increase with decreasing y_s.

challenging to capture within the presented computational framework because of a finite size of elements and locking effects. Thus, in the current study we limited ourselves to periodic wrinkling, period-doubling, and the transition into folds.

Figure 4c illustrates the effects of an exponential stiffness distribution in the subcortex on the surface morphology for two different stiffness ratios at the cortical-subcortical interface, $(\mu_c/\mu_s)_0 = 5$ and $(\mu_c/\mu_s)_0 = 10$. With increasing y_s from left to right we observe a notable increase in the folding wavelength accompanied by slightly increasing folding amplitudes. With increasing stiffness ratio at the cortical-subcortical interface from top to bottom, the cortical wavelength only shows a slight increase, but the maximum folding amplitudes grow recognizably larger before transitioning into folds by forming self-contact.

Figure 5 illustrates the influence of an exponentially increasing substrate stiffness on the final folding morphology in Figure 5a and the critical growth in Figure 5b of a three-dimensional ellipsoid. We assume axial symmetry and only simulate an eighth of the hollow ellipsoid discretized by 12936 elements with 43539 degrees of freedom. Because of the heterogeneous curvature of the ellipsoid, no additional perturbation is necessary to consistently initiate folding. We evaluate the $d\bar{t}_c/d\vartheta$ evolution to reliably determine the critical growth for the wrinkling instability. Similar to the results of the two-dimensional simulation domain, the critical wavelength increases with increasing stiffness contrast at the cortical-subcortical interface $(\mu_c/\mu_s)_0$ and increasing y_s, while the critical growth decreases asymptotically with increasing stiffness contrast and increases with decreasing y_s. However, critical growth values are generally slightly higher than on a rectangular simulation domain, which agrees with previous studies showing that the critical growth increases with increasing curvature [18, 10]. It also becomes apparent that, even for a comparably high stiffness contrast of $(\mu_c/\mu_s)_0 = 12$, in the right column of Figure 5, we observe realistic folding patterns in the analyzed parameter range. On a substrate with uniform stiffness, in contrast, a stiffness contrast of 12 would evoke unrealistic folding morphologies, where folds grow significantly before forming self contact [11]. The final folding patterns for the parameter sets $(\mu_c/\mu_s)_0 = 3$ and $y_s = 8$ in the bottom row of the first column, and $(\mu_c/\mu_s)_0 = 12$ and $y_s = 2$ in the middle row of the last column appear very similar, which agrees with the theoretically predicted wavelengths in Figure 4a. However, for the latter, the cortex buckles at a lower growth ϑ_w.

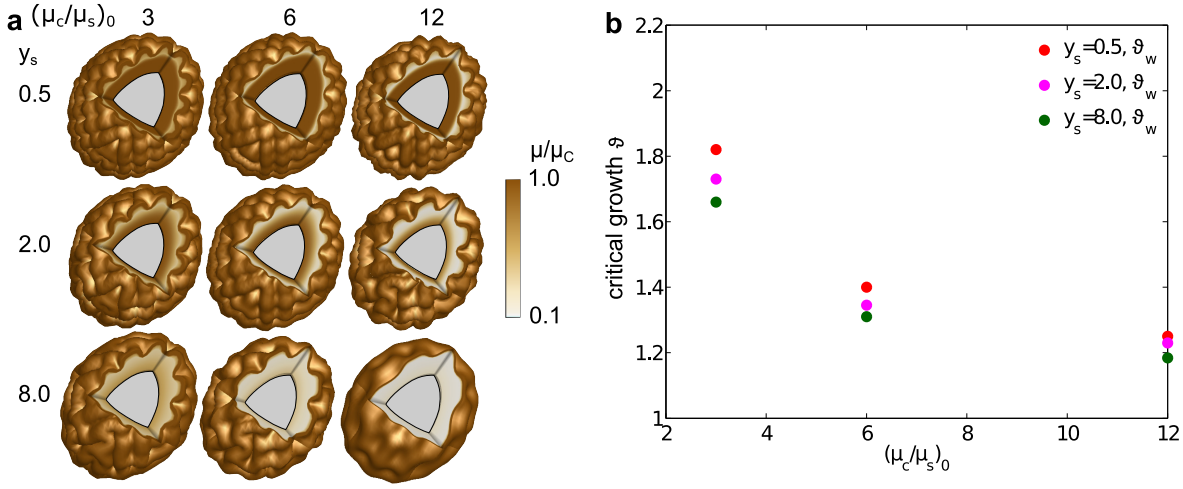

Figure 5: Sensitivity of surface morphology (a) and critical growth (b) with respect to stiffness gradient in the substrate and stiffness contrast $(\mu_c/\mu_s)_0$ at the cortical-subcortical interface on an ellipsoidal simulation domain. The critical wavelength increases with increasing stiffness contrast and increasing y_s. The critical growth ϑ_w decreases asymptotically with increasing stiffness contrast and increases with decreasing y_s.

3.3. Inhomogeneous stiffness in the cortex

The developing cortex has a thickness of only a few millimeters. Furthermore, the potential stiffness differences due to the radial gradient in neuronal maturation from the inside to the outside might partially be cancelled out by the network of blood vessels entering the brain from the outer surface to provide cells with nutrition and oxygen. Thus, we suppose that stiffness differences in the radial direction are minor. However, the cortical stiffness may vary in the tangential direction, when functional demands lead to variations in cell maturation and connectivity. This is supported by recent experimental evidence revealing that brain stiffness correlates with the fractional anisotropy (FA) obtained from diffusion magnetic resonance imaging as a measure of morphological complexity of brain cells and their connections. This observation has also opened new pathways to estimate stiffness distributions in the living fetal brain. A recent study on the fetal rhesus macaque brain, for instance, has provided evidence for spatial variations in cortical FA at the time when gyrification begins [50]. To investigate the influence of a non-uniform stiffness in the developing fetal cortex on the emerging folding pattern, we impose a sinusoidal stiffness distribution along the x-direction of the cortex on a two-dimensional rectangular simulation domain. We choose a periodicity of multiples of the characteristic folding wavelength for uniform material properties $\lambda^{\text{crit, uni}}$, which would occur if the stiffness was constant at its mean value. To emphasize the effects of cortical stiffness, we assume the substrate stiffness to be homogeneous. We choose a domain width of 14 times the characteristic wavelength $\lambda^{\text{crit, uni}}$, a maximum stiffness contrast of $(\mu_c/\mu_s)_{\text{max}} = 5$, and a minimum value of $(\mu_c/\mu_s)_{\text{min}} = 1$.

Figure 6 shows the influence of an inhomogeneous stiffness distribution along the cortical axis on the folding morphology. For illustrative purposes, we only show half of the simulation domain. Interestingly, both critical wavelength and critical growth appear independent of the tangential stiffness distribution in the cortex as long as the mean stiffness remains constant. However, the non-uniform stiffness controls the location of sulci and gyri and evokes a slightly irregular folding morphology. For such irregular patterns, the evolution of the mean cortical thickness provides a convenient tool to identify critical conditions for growth-induced instabilities.

3.4. Inhomogeneous cortical growth

The deep proliferating zones in the developing brain, where migrating cells originate from, are thicker beneath gyri and thinner beneath sulci as indicated in Figure 7 [33, 35]. We suppose that more cells migrate at sites of thicker proliferating zones associated with higher growth rates G_c. As morphological complexity of cortical neurons correlates with brain function, areas with higher functional demands most likely grow faster than less involved areas. These assumptions are supported by the fact that the developing cortex is thicker in the crowns of gyri and thinner in sulci [55]. To investigate to which extent regional variations in the growth rate a priori determine the location of gyri and sulci, we systematicly study the influence of non-uniform cortical growth rates on the emerging folding pattern. Similar to the setup in Section 3.3, we impose a sinusoidal distribution of the growth rates $G_c(x)$ with wavelengths of λ^G =0.25, 0.50, 1.00, 1.50, 2.00, and 3.00 times the characteristic wavelength $\lambda^{\text{crit, uni}}$ and compare the emerging pattern with uniform cortex growth as assumed in most previous studies [11, 47]. The minimum growth rate is $0.5\,G_{\text{c, uni}}$ and the maximum rate $1.5\,G_{\text{c, uni}}$ with the uniform growth rate $G_{\text{c, uni}}$. To solely focus on the effects of nonuniform cortical growth, we assume homogeneous stiffness in the cortex and subcortex, respectively, with a stiffness contrast $(\mu_c/\mu_s)_{\text{max}} = 5$.

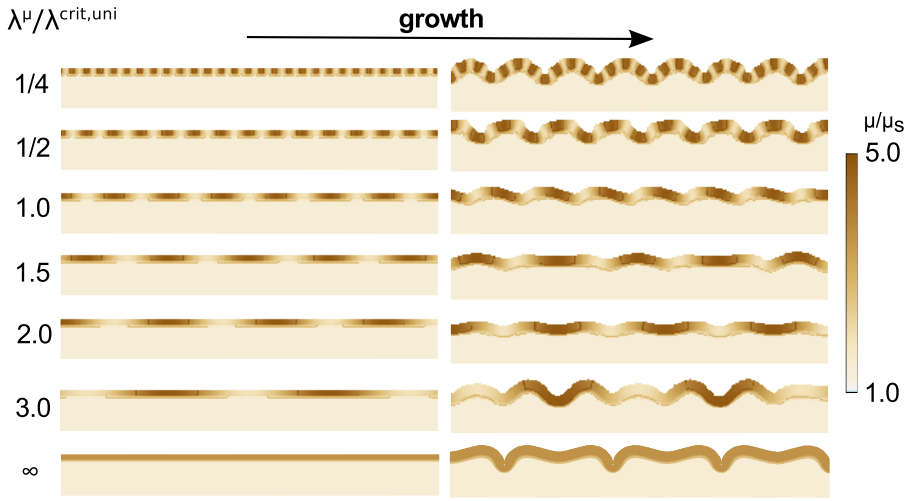

Figure 6: Influence of locally varying cortical stiffness on the evolution of the folding pattern. The contrast between the wavelength of the imposed stiffness pattern and the characteristic wavelength $\lambda^{\mu}/\lambda^{\text{crit, uni}}$ increases from top to bottom. The inhomogeneous cortical stiffness controls the location of sulci and gyri, but not the wavelength of folds.

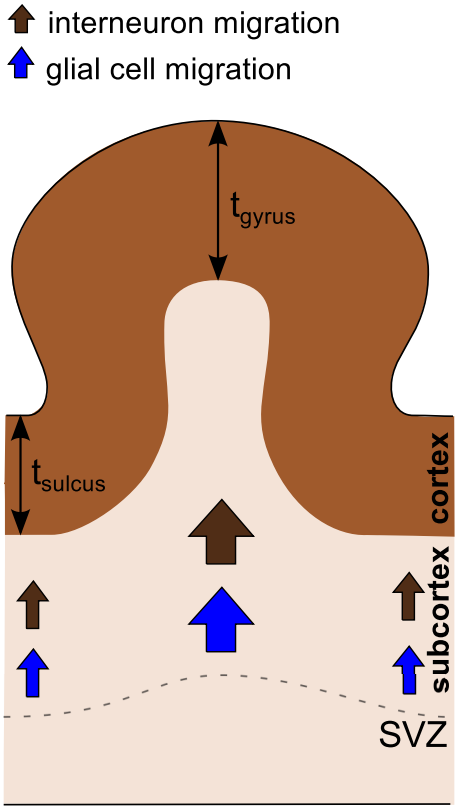

Figure 7: Cellular processes during brain development. Neurons and glial cell migrate outward from deep proliferating zones, the ventricular zone (VZ) and the subventricular zone (SVZ), to form the cortex. The SVZ is thicker beneath developing gyri and thinner beneath developing sulci. Also the cortex is thicker in gyri than in sulci.

Figure 8 shows the evolution of the folding pattern for sinusoidally distributed growth rates in the cortex. As the cortex grows isotropically, regionally varying cortical growth does not only result in an inhomogeneous cortical pressure but also in an inhomogeneous cortical thickness. As a result, the surface morphology appears as a wavy pattern even prior to the onset of wrinkling, which later bifurcates into the pattern associated with the instability. When λ^{G} is within a certain band around the characteristic wavelength $\lambda^{\text{crit, uni}}$, the imposed pattern prevails as shown in rows 3 to 5 in Figure 8. The deepening of the mechanically weakest, thinnest locations is sufficient to release the growth-induced compression in the cortex. This observation

can be associated with a well known phenomenon in convection: according to the Eckhaus instability, patterns can be stable within a certain band around the characteristic wavelength [1]. When the imposed pattern is significantly different from the characteristic pattern, however, the cortex bifurcates into wrinkles with the characteristic wavelength. The surface pattern initially established from local differences in cortical growth and thickness would not sufficiently release cortical compression. This becomes apparent in rows 1, 2, 6, and 7 in Figure 8, where the coloring does not coincide with the emerging folding pattern. For $\lambda^{\mathrm{G}}/\lambda^{\mathrm{crit,\,uni}} = 3.0$ shown in the 6th row of Figure 8, for instance, all gyri in the middle column have transformed into sulci in the right column. Not surprisingly, the local variations in cortical growth control the location of sulci and induce irregular folding patterns. The deepest sulci will form where the cortex is thinnest. When we impose the characteristic wavelength $\lambda^{\mathrm{G}}/\lambda^{\mathrm{crit,\,uni}} = 1.0$, we simply cause a horizontal shift of gyri and sulci according to the local thickness differences. Interestingly, though, the secondary instability changes: wrinkles transition into folds before the onset of period-doubling. We further note that while both $\lambda^{\mathrm{G}}/\lambda^{\mathrm{crit,\,uni}} = 2.0$ and $\lambda^{\mathrm{G}}/\lambda^{\mathrm{crit,\,uni}} = \infty$ reveal a period-doubling pattern in the right column of Figure 8, only the latter originates from a secondary instability.

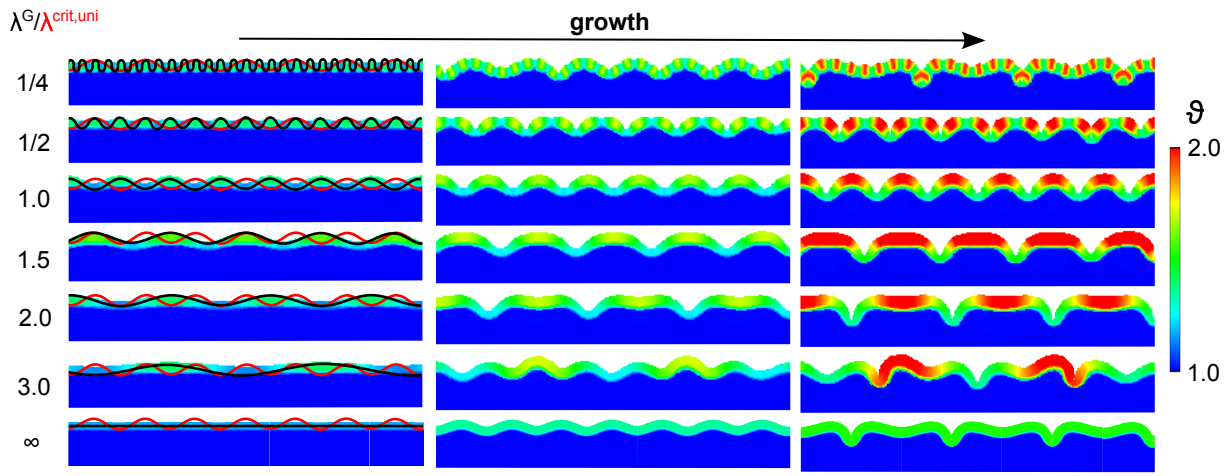

Figure 8: Influence of locally varying cortical growth rates on the evolution of the folding pattern. The ratio between the wavelength of the imposed growth pattern and the characteristic wavelength increases from top to bottom with $\lambda^{\mathrm{G}}/\lambda^{\mathrm{crit,\,uni}} = 0.25, 0.50, 1.00, 1.50, 2.00, 3.00$, and ∞.

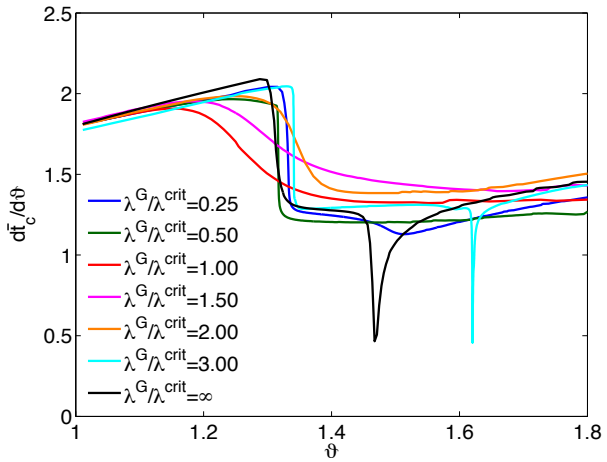

Figure 9: Evolution of the rate of change of the mean cortical thickness $\mathrm{d}\bar{r}_{\mathrm{c}}/\mathrm{d}\vartheta$ as a function of growth ϑ for imposed growth patterns of 0.25, 0.50, 1.00, 1.50, 2.00, and 3.00 times the characteristic wavelength $\lambda^{\mathrm{crit,\,uni}}$ as well as uniform growth. A drop in $\mathrm{d}\bar{r}_{\mathrm{c}}/\mathrm{d}\vartheta$ initiates the primary instability, where the surface buckles into sinusoidal wrinkles.

Figure 9 shows the evolution of the rate of change of mean cortical thickness $\mathrm{d}\bar{r}_{\mathrm{c}}/\mathrm{d}\vartheta$ with growth. Before initiation of the primary instability, the cortex thickens faster than after the first instability point associated with a higher rate $\mathrm{d}\bar{r}_{\mathrm{c}}/\mathrm{d}\vartheta$. When the

imposed growth pattern is significantly different from the characteristic pattern and the characteristic wavelength will prevail, we can uniquely determine the critical growth for the onset of wrinkling ϑ_w. For, $\lambda^{\mathrm{G}}/\lambda^{\mathrm{crit,uni}} = 1.00, 1.50$ and 2.00, in contrast, we observe a smooth transition from the unbuckled to the buckled configuration. The closer λ^{G} and $\lambda^{\mathrm{crit,uni}}$, the earlier the instability will set in. Notably, while sinusoidally varying growth rates affect the location or even wavelength of folds, the primary critical growth value remains almost constant. Non-uniform growth patterns lead to a slight increase of ϑ_w. The $\mathrm{d}\bar{t}_c/\mathrm{d}\vartheta$ evolutions further indicate that the secondary instability is even more sensitive to non-uniform growth patterns than the primary instability. Imposing a sinusoidal growth distribution clearly delays the onset of period-doubling or even completely suppresses the emergence of the secondary instability. It will only occur when the imposed pattern is significantly different from the characteristic pattern, for instance for $\lambda^{\mathrm{G}}/\lambda^{\mathrm{crit,uni}} = 0.25$ or 3.0. Though, the secondary instability point is shifted towards higher growth compared to uniform growth.

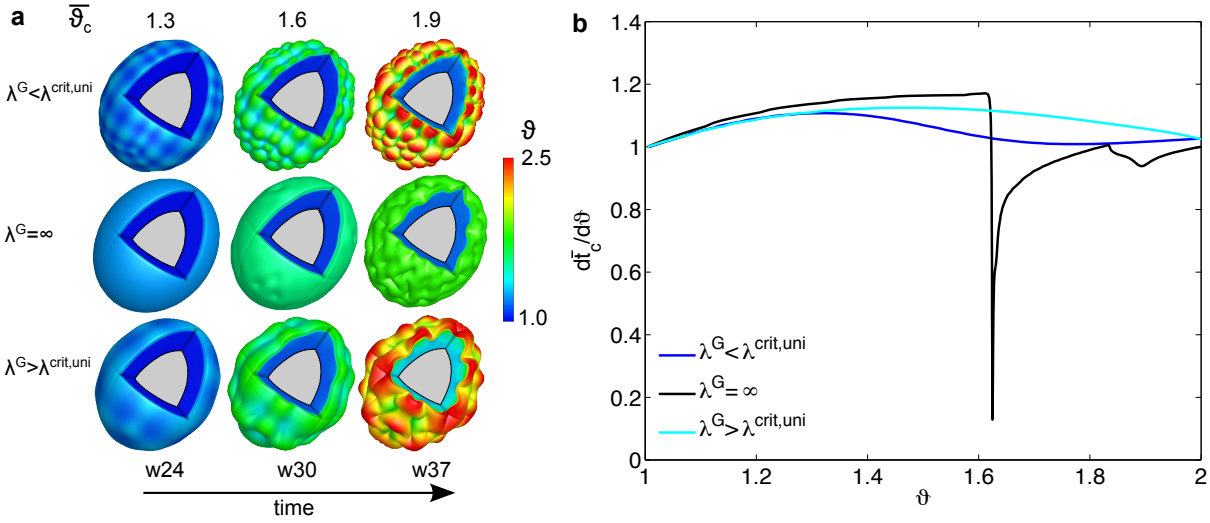

Figure 10: Influence of locally varying cortical growth rates on the evolution of the folding pattern on a three-dimensional ellipsoidal simulation domain.

Figure 10 illustrates the effects of non-uniform cortical growth on the evolving patterns on a three-dimensional ellipsoidal simulation domain. Similar to the results on the two-dimensional domain, in the top row, a growth pattern with a slightly lower wavelength than the characteristic pattern $\lambda^{\mathrm{G}} < \lambda^{\mathrm{crit,uni}}$ is adopted, whereas in the bottom row, the imposed wavelength is not sufficient to release cortical compression and the initial gyri at the edges of the domain fold inwards to become sulci after the instability point. Again, we see a smooth transition from the unbuckled to the buckled state. For uniform growth, the $\mathrm{d}\bar{t}_c/\mathrm{d}\vartheta$ evolution indicates a secondary instability, but for inhomogeneous growth patterns, neighboring folds form self-contact before a secondary instability would set in.

4. Discussion

Despite their importance for proper brain functioning, the underlying mechanisms of cortical folding during brain development have long remained understudied and not well understood [4]. After the phenomenon of brain folding has attracted the attention of physicists and engineers, more and more evidence suggests that mechanical instabilities play a major role in pattern selection. The outer cortex grows tremendeously when cortical neurons mature and form connections; the constraint of the slower growing inner subcortex leads to compression in the cortex and surface buckling [40, 3, 11, 46, 39, 47]. Previous studies on the mechanical factors during brain development have mostly assumed homogeneous material and growth properties within the two different layers. In this study, we have shown that not only cortical thickness, the stiffness contrast between cortex and subcortex, and geometry, but also the inhomogeneous character of properties generally known for biological tissues affects growth-induced instabilities. Such inhomogeneities represent an additional factor which needs to be taken into account when aiming to predict and understand cortical folding during brain development. We have approximated stiffness and growth distributions based on mechanisms on the cellular level and studied their influence on the evolving pattern. The current study emphasizes the importance of the characteristic wavelength - a quantity well known from linear perturbation analyses. Mechanically weak spots in the developing brain control the location of sulci and gyri and lead to irregular folding patterns but the cortical wavelength is remarkably stable against inhomogeneities.

4.1. Geometrical quantities reveal the characteristics of growth-induced instabilities at the onset of wrinkling and beyond

The computational framework presented in the current study allows us to determine the critical wavelength and growth for primary wrinkling and to investigate growth-induced instabilities in the post-buckling regime or for highly perturbed systems,

where we observe a smooth transition from the unwrinkled to the wrinkled state. We have demonstrated that geometrical quantities, the evolution of amplitudes and mean cortical thickness as well as their derivatives with respect to growth, enable us to reliably determine the critical growth for primary and secondary instabilities. In contrast to the folding amplitude, the mean cortical thickness is a quantity accessible in highly inhomogeneous systems, where sulci and gyri are not stable with growth as illustrated in the 6th row of Figure 8. It allows us to detect the point of the instability on irregular three-dimensional geometries in Figures 5 and 10. Furthermore, the derivative of mean cortical thickness with respect to growth reveals that the increase in thickness slows down after the primary instability, but not after the secondary instability. This indicates that primary periodic wrinkling minimizes compression in the cortex, while secondary period-doubling minimizes compression in the subcortex. This agrees well with theoretical considerations suggesting that secondary instabilities are highly associated with substrate non-linearity [30]. It also explains why the secondary critical growth is independent of the stiffness contrast at the cortical-subcortical interface for a non-growing substrate or for $(\mu_c/\mu_s)_0 \to 1$. In contrast, the stiffness distribution in the substrate, which we parameterize by y_s, does affect the secondary critical condition as shown in Figure 4 and discussed in the next paragraph. The characterization of mechanical instabilities through geometrical quantities is not only relevant for biological tissues, which are naturally highly heterogeneous, but also for advanced technical structures such as functionally graded materials [15, 53, 54].

4.2. Radial stiffness gradient in the developing subcortex

While it is possible to obtain analytical estimates for the critical wavelength and growth at the onset of buckling for graded substrate stiffnesses following a simple exponential function converging towards zero for $y \to \infty$ [15], the distribution we deduce from the microstructure in the developing brain, equation (8), requires numerical treatment [36]. When the subcortex stiffens with depth, critical wavelengths for primary wrinkling are shorter compared to the homogeneous case and the critical growth increases. With continuing growth, periodic wrinkles bifurcate into period-doubles as the favorable secondary mode. For a homogeneous, non-growing substrate it has been shown that the secondary critical growth ϑ_{pd} is independent of the stiffness contrast μ_c/μ_s [7]. For an inhomogeneous, non-growing substrate, ϑ_{pd} does not depend on the stiffness contrast at the cortical-subcortical interface $(\mu_c/\mu_s)_0$ but on the stiffness distribution in the substrate quantified by the parameter y_s. The critical growth for period-doubling ϑ_{pd} increases as y_s decreases as illustrated in Figure 4; the faster the subcortical white matter stiffens with depth, the higher ϑ_{pd}. In addition, the stretch-induced growth response of the subcortex [11] leads to an increase in ϑ_{pd} for longer wavelength and higher folding amplitudes as $(\mu_c/\mu_s)_0$ and y_s increase [13]. Simulating on a three-dimensional ellipsoidal simulation domain reveals that even for relatively high stiffness contrasts at the cortical-subcortical interface $(\mu_c/\mu_s)_0$, the surface morphology quite well resembles the one of mammalian brains. For a homogeneous substate, in contrast, high stiffness contrasts lead to unrealistic morphologies, where gyri grow significantly without forming self-contact [11]. This can be attributed to the fact that the morphology of folds tends towards a more crease-like shape with cusped sulci when the stiffness contrast approaches one [46]. Of all simulated parameters, we expect a stiffness decay of $y_s \approx 2$ and a stiffness contrast $(\mu_c/\mu_s)_0$ between 3 and 6 to be most realistic for the human brain in its early stage of development.

4.3. Tangentially varying stiffness distribution in the developing cortex

Motivated by spatial variations in cell migration and maturation of the cortex, we have investigated the influence of periodically varying cortical stiffness on the critical growth for growth-induced instabilities and the emerging folding pattern. We have shown that the critical wavelength and growth values conform to the mean stiffness. When we altered the period length of the stiffness distribution but kept the mean stiffness constant, critical wavelength and growth remained unchanged. Interestingly, a recent study on inhomogeneous film-on-substrate systems revealed that a ramp-like variation in substrate stiffness narrows the band of stable wavelengths compared to a step-like change in stiffness [1]. Thus, although unexpected in the developing brain, step-like changes in tissue stiffness could more likely affect the folding wavelength as a wider range of patterns would be stable. Our numerical investigations have further revealed that inhomogeneous cortical stiffness controls the location of sulci and gyri and evokes irregular surface patterns. Our findings agree well with a recent computational study showing that locally stiffened areas in the developing cortex always lead to sulci formation [55]. Interestingly, also a longitudinal study on fractional anisotropy (FA) in the fetal rhesus macaque cortex [50] as a measure of morphological complexity of brain cells and their connections - and thus an indicator for tissue stiffness [9] - confirms that deepest sulci form at locations of lowest FA corresponding to highest stiffness. The FA distributions seem to determine the locations of deep sulci but seem not to have a marked effect on the cortical wavelength as predicted by our simulations in Section 3.3. The irregularity of the simulated surface patterns in Figure 6 is also consistent with recent experimental studies showing that a periodic stiffness distribution of a hardened skin layer on a soft material can create various micropatterns [49] with non-uniform undulating surface features [53].

4.4. Tangentially varying growth distribution in the developing cortex

Motivated by the observation that proliferating zones, where cortical neurons originate from, are thinner beneath sulci and thicker beneath gyri [44], we suppose that cortical growth shows spatial variations. Thus, we have investigated the influence of periodically varying growth rates on the evolving folding pattern. When the period length of the growth pattern lies within a certain

range around the characteristic wavelength, the imposed pattern can be stable and prevail as shown in row three and four of Figure 8. We observe a smooth transition from the unbuckled to the buckled state. This can be pulled together with the fact that a central property of nonlinear periodic patterns is that at a given set of parameters not only a single wavelength may be stable, but all wavelengths within the so-called Eckhaus stability bands [22, 34, 1]. In contrast, when the period length of the growth pattern is significantly different from the characteristic wavelength, the surface bifurcates into the characteristic pattern at the well defined critical growth value. We conclude that the final wavelength of folds will always be within a small band around the characteristic wavelength predicted from theoretical or numerical analyses.

Interestingly, inhomogeneous cortical growth rates evoke irregular patterns with non-uniform amplitudes that might also resemble secondary folding patterns such as period-doubling as shown in the fifth row of Figure 8. This emphasizes that besides secondary bifurcations [13], and irregular geometries [47], inhomogeneities in cortical growth represent an additional source of irregular surface patterns. This agrees with studies showing that controlled thickness gradients create irregular wrinkling patterns in metal films on soft substrates [53, 54]. During secondary wrinkling instabilities the location and number of sulci and gyri stays constant. But for inhomogeneous growth rates, the initially evolving morphology might be superimposed by the characteristic pattern after the onset of wrinkling (compare the left column with the middle and right column in Figure 8): additional sulci fold inwards. This is an interesting difference between those two phenomena, which is indeed observed in the developing human brain: First well identified primary gyri evolve separated by shallow sulci; this is then followed by further infolding of the brain surface during secondary and tertiary folding [42]. We thus presume that the well preserved primary folds occur at locations of locally thinned cortices or slow growth rates similar to the left column of Figure 8, while highly variable secondary folds are not only associated with secondary bifurcations but also with primary bifurcations of an inhomogeneously growing system. This theory could also explain why the sulcal pattern becomes more consistent at increasing depths below the surface [37]. Our results are consistent with a recent computational study showing that a gyrus will form in areas of higher growth rates [55]. We conclude that an interplay of the infolding of mechanically weak spots and growth-induced instabilities shape the developing brain with primary folds that are consistent between individuals and highly variable secondary and tertiary folds. We note that the effect of tangentially varying growth rates would have been slightly less pronounced if we had assumed area growth instead of isotropic growth in the cortex [3, 47], where inhomogeneous growth does not result in inhomogeneous cortical thickness. However, according to a recent study combining experimental and computational data, isotropic growth seems to more realistically resemble growth in the developing human brain [55].

4.5. How to classify growth-induced instabilities in the developing fetal brain

Although different mechanisms could lead to final secondary morphologies, the underlying mechanisms become apparent when detecting the evolution of cortical thickness and folding amplitudes with growth. Modern magnetic resonance technologies have opened new paths in tracking the surface morphology of the fetal brain in vivo [27]. With further enhancement of such imaging techniques, it might be possible to accurately record the thickness of the developing cortical layer over time. Then, the presented approach will enable us to finally answer the question whether it is indeed growth-induced mechanical instabilities underlying cortical folding.

4.6. Limitations

In this study, we have assumed that growth and stiffness distributions are constant in time. However, this is not necessarily the case in the highly dynamic developing brain. A recent longitudinal study on the fractional anisotropy in the fetal macaque cortex, for instance, indicates that the tangential stiffness distribution changes over time [50, 9]. Furthermore, fetal brain tissue in general has been shown to be softer than mature brain tissue [51]. Regarding cellular processes during brain development, we suppose that gray matter stiffens earlier than white matter which might lead to a slight increase in the stiffness ratio throughout the folding process. However, the primary pattern only depends on the conditions at the onset of folding which we tried to imitate based on cellular mechanisms in the current study. Once established, neither a tangential shift in the cortical stiffness distribution nor a moderate increase in the stiffness ratio will affect the location of sulci and gyri. On the one hand, wavelengths can be stable within a certain band around the characteristic wavelength, when growth has exceeded the primary instability point ϑ_w as discussed in Section 4.4 [1]. On the other hand, the characteristic wavelength for tangentially varying cortical stiffness is determined by its mean value, which is not affected by a mere redistribution. Still, temporal variations in properties could affect the post-buckling evolution of the folding morphology and the irregularity of the surface pattern [23]. With post-critically increasing stiffness ratio, sulci become more shallow and folding amplitudes grow significantly before they form self-contact. This effect, however, only becomes noticeable for a significant increase in cortical stiffness, which seems unphysiological for brain tissue. In the current study we further focused on stiffness contrasts at the cortical-subcortical interface $(\mu_c/\mu_s)_0$ in the range of 3 and 12. When μ_c/μ_s <1.14 [45], cusped sulci will form instead of sinusoidal wrinkles which immediately tranform into folds, also referred to as creases [46, 45]. In this case, there is not necessarily a single wavelength favored for folding [29]. While the stiffness difference between gray and white matter in the developing brain is still under debate [19, 48], recent experiments indicate that $(\mu_c/\mu_s)_0 \geq 1$ at very slow loading rates (relevant for growth processes). Elastic properties seem to correlate with connectivity and capillary density [9]. As the cortex maturates

well before the white matter, we expect that the stiffness contrast between cortex and subcortex in early stages of development is generally even larger than in the fully developed brain with $\mu_c/\mu_s \approx 2.15$ [9]. Locally, however, a similar stiffness in cortex and subcortex could lead to the formation of creases rather than folds, especially in later stages of cortical folding (tertiary folding). For a detailed study on the transition from supercritical smooth wrinkling to subcritical cusped folding, we refer to [45]. Lastly, we use linear finite elements which have been shown to lead to slight deviations when computing the critical growth to initiate instabilities [31]. While such numerical inaccuracies are irrelevant in the context of brain folding, in technical systems where slight differences could decide about failure, quadratic finite elements should be used.

5. Conclusion

Through computational analyses, we have shown how inhomogeneities in stiffness and growth arising from the highly dynamic cellular processes during brain development control emerging surface patterns. We have demonstrated that geometrical quantities including the evolution of amplitudes and mean cortical thickness imply important characteristics of growth-induced primary and secondary instabilities. Characteristic wavelength and critical growth depend on the stiffness distribution in the subcortex but are remarkably stable towards heterogeneous cortical growth. The latter, however, can evoke highly irregular surface morphologies mistakable with secondary wrinkling patterns. Our results suggest that well preserved primary folds occur at locations of locally thinned cortices or slow growth rates, while highly variable secondary and tertiary folds evolve from primary and secondary growth-induced instabilities. This study paves the way towards analyzing growth-induced instabilities from geometrical data of the living fetal brain obtained with the rapidly advancing imaging techniques.

Acknowledgements

This study was kindly supported by the German National Science Foundation grant STE 544/50 to Silvia Budday and Paul Steinmann, the Cluster of Excellence Engineering of Advanced Materials (EAM) to Paul Steinmann, and by the Humboldt Research Award to Ellen Kuhl. We further thank Sebastian Andres for stimulating discussions.

References

[1] R. Aichele, B. Kaoui, F. Ziebert, and W. Zimmermann. Branched wrinkles in inhomogeneous film-on-substrate systems. *submitted*, 2017.

[2] M. B. Amar and A. Goriely. Growth and instability in elastic tissues. *Journal of the Mechanics and Physics of Solids*, 53(10):2284–2319, 2005.

[3] P. Bayly, R. Okamoto, G. Xu, Y. Shi, and L. Taber. A cortical folding model incorporating stress-dependent growth explains gyral wavelengths and stress patterns in the developing brain. *Physical biology*, 10(1):016005, 2013.

[4] P. Bayly, L. Taber, and C. Kroenke. Mechanical forces in cerebral cortical folding: a review of measurements and models. *Journal of the mechanical behavior of biomedical materials*, 29:568–581, 2014.

[5] M. Biot. Folding instability of a layered viscoelastic medium under compression. In *Proceedings of the Royal Society of London A: Mathematical, Physical and Engineering Sciences*, volume 242, pages 444–454. The Royal Society, 1957.

[6] D. Bray. Axonal growth in response to experimentally applied mechanical tension. *Developmental biology*, 102(2):379–389, 1984.

[7] S. Budday, E. Kuhl, and J. W. Hutchinson. Period-doubling and period-tripling in growing bilayered systems. *Philosophical Magazine*, 95:3208–3224, 2015.

[8] S. Budday, C. Raybaud, and E. Kuhl. A mechanical model predicts morphological abnormalities in the developing human brain. *Scientific reports*, 4, 2014.

[9] S. Budday, G. Sommer, C. Birkl, C. Langkammer, J. Haybaeck, J. Kohnert, M. Bauer, F. Paulsen, P. Steinmann, E. Kuhl, et al. Mechanical characterization of human brain tissue. *Acta biomaterialia*, 48:319–340, 2017.

[10] S. Budday, P. Steinmann, A. Goriely, and E. Kuhl. Size and curvature regulate pattern selection in the mammalian brain. *Extreme Mechanics Letters*, 4:193–198, 2015.

[11] S. Budday, P. Steinmann, and E. Kuhl. The role of mechanics during brain development. *Journal of the Mechanics and Physics of Solids*, 72:75–92, 2014.

[12] S. Budday, P. Steinmann, and E. Kuhl. Physical biology of human brain development. *Frontiers in cellular neuroscience*, 9, 2015.

[13] S. Budday, P. Steinmann, and E. Kuhl. Secondary instabilities modulate cortical complexity in the mammalian brain. *Philosophical Magazine*, 95:3244–3256, 2015.

[14] I. Bystron, C. Blakemore, and P. Rakic. Development of the human cerebral cortex: Boulder committee revisited. *Nature Reviews Neuroscience*, 9(2):110–122, 2008.

[15] Y.-P. Cao, F. Jia, Y. Zhao, X.-Q. Feng, and S.-W. Yu. Buckling and post-buckling of a stiff film resting on an elastic graded substrate. *International Journal of Solids and Structures*, 49(13):1656–1664, 2012.

[16] S. Chatelin, J. Vappou, S. Roth, J.-S. Raul, and R. Willinger. Towards child versus adult brain mechanical properties. *Journal of the mechanical behavior of biomedical materials*, 6:166–173, 2012.

[17] F. Chen, J. Zhou, Y. Li, Y. Wang, L. Li, and H. Yue. Mechanical properties of porcine brain tissue in the coronal plane: Interregional variations of the corona radiata. *Annals of biomedical engineering*, 43(12):2903–2910, 2015.

[18] X. Chen and J. Yin. Buckling patterns of thin films on curved compliant substrates with applications to morphogenesis and three-dimensional micro-fabrication. *Soft Matter*, 6(22):5667–5680, 2010.

[19] A. F. Christ, K. Franze, H. Gautier, P. Moshayedi, J. Fawcett, R. J. Franklin, R. T. Karadottir, and J. Guck. Mechanical difference between white and gray matter in the rat cerebellum measured by scanning force microscopy. *Journal of biomechanics*, 43(15):2986–2992, 2010.

[20] W. L. G. Clark. *Essays on growth and form*, chapter Deformation patterns in the cerebral cortex. Oxford University Press, London, 1945.

[21] T. J. Dennerll, P. Lamoureux, R. E. Buxbaum, and S. R. Heidemann. The cytomechanics of axonal elongation and retraction. *The journal of cell biology*, 109(6):3073–3083, 1989.

[22] W. Eckhaus. *Studies in Nonlinear Stability Theory*, volume 6 of *Springer Tracts in Natural Philosophy*. Springer Berlin Heidelberg, 1965.

[23] M. Eskandari, A. Javili, and E. Kuhl. Elastosis during airway wall remodeling explains multiple co-existing instability patterns. *Journal of theoretical biology*, 403:209–218, 2016.

[24] G. Fallenstein, V. D. Hulce, and J. W. Melvin. Dynamic mechanical properties of human brain tissue. *Journal of Biomechanics*, 2(3):217–226, 1969.

[25] G. Franceschini, D. Bigoni, P. Regitnig, and G. A. Holzapfel. Brain tissue deforms similarly to filled elastomers and follows consolidation theory. *Journal of the Mechanics and Physics of Solids*, 54(12):2592–2620, 2006.

[26] K. Garikipati. The kinematics of biological growth. *Applied Mechanics Reviews*, 62(3):030801, 2009.

[27] P. A. Habas, J. A. Scott, A. Roosta, V. Rajagopalan, K. Kim, F. Rousseau, A. J. Barkovich, O. A. Glenn, and C. Studholme. Early folding patterns and asymmetries of the normal human brain detected from in utero mri. *Cerebral cortex*, 22(1):13–25, 2012.

[28] E. Hohlfeld and L. Mahadevan. Unfolding the sulcus. *Physical review letters*, 106(10):105702, 2011.

[29] M. Holland, B. Li, X. Feng, and E. Kuhl. Instabilities of soft films on compliant substrates. *Journal of the Mechanics and Physics of Solids*, 98:350–365, 2017.

[30] J. W. Hutchinson. The role of nonlinear substrate elasticity in the wrinkling of thin films. *Philosophical Transactions of the Royal Society of London A: Mathematical, Physical and Engineering Sciences*, 371(1993):20120422, 2013.

[31] A. Javili, B. Dortdivanlioglu, E. Kuhl, and C. Linder. Computational aspects of growth-induced instabilities through eigenvalue analysis. *Computational Mechanics*, 56(3):405–420, 2015.

[32] A. Javili, P. Steinmann, and E. Kuhl. A novel strategy to identify the critical conditions for growth-induced instabilities. *Journal of the Mechanical Behavior of Biomedical Materials*, 29:20–32, 2014.

[33] I. Kostović, M. Judaš, M. Radoš, and P. Hrabač. Laminar organization of the human fetal cerebrum revealed by histochemical markers and magnetic resonance imaging. *Cerebral Cortex*, 12(5):536–544, 2002.

[34] L. Kramer and W. Zimmermann. On the eckhaus instability for spatially periodic patterns. *Physica D: Nonlinear Phenomena*, 16(2):221–232, 1985.

[35] A. Kriegstein, S. Noctor, and V. Martínez-Cerdeño. Patterns of neural stem and progenitor cell division may underlie evolutionary cortical expansion. *Nature Reviews Neuroscience*, 7(11):883–890, 2006.

[36] D. Lee, N. Triantafyllidis, J. Barber, and M. Thouless. Surface instability of an elastic half space with material properties varying with depth. *Journal of the Mechanics and Physics of Solids*, 56(3):858–868, 2008.

[37] G. Lohmann, D. Y. von Cramon, and H. Steinmetz. Sulcal variability of twins. *Cerebral Cortex*, 9(7):754–763, 1999.

[38] C. Raybaud, T. Ahmad, N. Rastegar, M. Shroff, and M. Al Nassar. The premature brain: developmental and lesional anatomy. *Neuroradiology*, 55(2):23–40, 2013.

[39] M. J. Razavi, T. Zhang, T. Liu, and X. Wang. Cortical folding pattern and its consistency induced by biological growth. *Scientific reports*, 5, 2015.

[40] D. P. Richman, R. M. Stewart, J. Hutchinson, and V. S. Cavincss Jr. Mechanical mode of brain convolutional deve lopment. *Science*, 189:18–21, 1975.

[41] L. Ronan, N. Voets, C. Rua, A. Alexander-Bloch, M. Hough, C. Mackay, T. J. Crow, A. James, J. N. Giedd, and P. C. Fletcher. Differential tangential expansion as a mechanism for cortical gyrification. *Cerebral Cortex*, 24(8):2219–2228, 2014.

[42] M. A. Rutherford. *MRI of the Neonatal Brain*. Gulf Professional Publishing, 2002.

[43] L. Shuck and S. Advani. Rheological response of human brain tissue in shear. *Journal of basic engineering*, 94(4):905–911, 1972.

[44] T. Sun and R. F. Hevner. Growth and folding of the mammalian cerebral cortex: from molecules to malformations. *Nature Reviews Neuroscience*, 15(4):217–232, 2014.

[45] T. Tallinen and J. S. Biggins. Mechanics of invagination and folding: Hybridized instabilities when one soft tissue grows on another. *Physical Review E*, 92(2):022720, 2015.

[46] T. Tallinen, J. Y. Chung, J. S. Biggins, and L. Mahadevan. Gyrification from constrained cortical expansion. *Proceedings of the National Academy of Sciences*, 111(35):12667–12672, 2014.

[47] T. Tallinen, J. Y. Chung, F. Rousseau, N. Girard, J. Lefèvre, and L. Mahadevan. On the growth and form of cortical convolutions. *Nature Physics*, 2016.

[48] J. Van Dommelen, T. Van der Sande, M. Hrapko, and G. Peters. Mechanical properties of brain tissue by indentation: interregional variation. *Journal of the mechanical behavior of biomedical materials*, 3(2):158–166, 2010.

[49] J. Wang, B. Li, Y.-P. Cao, X.-Q. Feng, and H. Gao. Wrinkling micropatterns regulated by a hard skin layer with a periodic stiffness distribution on a soft material. *Applied Physics Letters*, 108(2):021903, 2016.

[50] X. Wang, C. Studholme, P. L. Grigsby, A. E. Frias, V. C. C. Carlson, and C. D. Kroenke. Folding, but not surface area expansion, is associated with cellular morphological maturation in the fetal cerebral cortex. *Journal of Neuroscience*, 37(8):1971–1983, 2017.

[51] J. Weickenmeier, R. de Rooij, S. Budday, T. C. Ovaert, and E. Kuhl. The mechanical importance of myelination in the central nervous system. *Journal of the Mechanical Behavior of Biomedical Materials*, 2017.

[52] J. Weickenmeier, R. de Rooij, S. Budday, P. Steinmann, T. Ovaert, and E. Kuhl. Brain stiffness increases with myelin content. *Acta Biomaterialia*, 42:265–272, 2016.

[53] J. Yin and X. Chen. Elastic buckling of gradient thin films on compliant substrates. *Philosophical Magazine Letters*, 90(6):423–433, 2010.

[54] S. Yu, Y. Ni, L. He, and Q.-L. Ye. Tunable formation of ordered wrinkles in metal films with controlled thickness gradients deposited on soft elastic substrates. *ACS applied materials & interfaces*, 7(9):5160–5167, 2015.

[55] T. Zhang, M. J. Razavi, X. Li, H. Chen, T. Liu, and X. Wang. Mechanism of consistent gyrus formation: an experimental and computational study. *Scientific Reports*, 6, 2016.